Journal of
*Composites Science*

MDPI

*Article*

# Mechanical Properties of a Unidirectional Basalt-Fiber/Epoxy Composite

**David Plappert [1,*], Georg C. Ganzenmüller [1], Michael May [2] and Samuel Beisel [1]**

[1] Institute for Sustainable Systems Engineering, Albert-Ludwigs Universität Freiburg, 79100 Freiburg i. Br., Germany; georg.ganzenmueller@inatech.uni-freiburg.de (G.C.G.); samuel.beisel@inatech.uni-freiburg.de (S.B.)
[2] Fraunhofer Ernst-Mach-Institute for High-Speed Dynamics, EMI, 79100 Freiburg i. Br., Germany; michael.may@emi.fraunhofer.de
* Correspondence: david.plappert@inatech.uni-freiburg.de

Received: 23 June 2020; Accepted: 27 July 2020; Published: 29 July 2020


**Abstract:** High-performance composites based on basalt fibers are becoming increasingly available. However, in comparison to traditional composites containing glass or carbon fibers, their mechanical properties are currently less well known. In particular, this is the case for laminates consisting of unidirectional plies of continuous basalt fibers in an epoxy polymer matrix. Here, we report a full quasi-static characterization of the properties of such a material. To this end, we investigate tension, compression, and shear specimens, cut from quality autoclave-cured basalt composites. Our findings indicate that, in terms of strength and stiffness, unidirectional basalt fiber composites are comparable to, or better than epoxy composites made from E-glass fibers. At the same time, basalt fiber composites combine low manufacturing costs with good recycling properties and are therefore well suited to a number of engineering applications.

**Keywords:** basalt fibers; natural fibers; polymer-matrix composites (PMCs); mechanical properties; mechanical testing

## 1. Introduction

Modern basalt fibers are a suitable high performance reinforcement for polymer composites. The mechanical properties of unidirectional basalt fiber reinforced polymers (BFRP) are similar to, or better than E-glass fiber reinforced polymers (GFRP)—elongation and stress at break are comparable [1] while their Young's Modulus is higher by up to 35% [2]. BFRP is therefore believed to potentially bridge the gap between GFRP and carbon fiber reinforced polymers (CFRP) [3]. Compared to glass fiber composites, BFRP combines stiffness and strength with good fatigue resistance and better energy absorption characteristics [1,2].

In addition to their competitive mechanical properties, the resources for basalt fibers are globally available and they may be produced with comparatively low energy consumption on a lower price level than glass and, in particular, carbon fibers [4]. They are produced by means of a spinning process from molten volcanic basalt rock. This process is very similar to the production of glass fibers, but in the case of basalt, no additives are required. This reduces risk of exposition to toxic substances [5]. Hence, the production is more environmentally friendly [6]. The fibers have good chemical stability, in particular high corrosion resistance [7] and thermal stability; they are usable over a wide range of temperatures, from −200 °C up to 800 °C [8,9]. While fiber strength decreases above temperatures of ≈300 °C [10], basalt fibers feature higher thermal stability than glass fibers [11]. This offers advantages when it comes to recycling of the composite, as long fibers may be recovered by pyrolitic removal of the matrix [5,12].

The chemical composition of basalt is dominated by $SiO_2$ with 42–56% (by weight), followed by $Al_2O_3$ (14–18%), $Fe_2O_3$ (11–12%), CaO (7–9%) and further oxides, depending on geological origin, see Figure 1 [13].

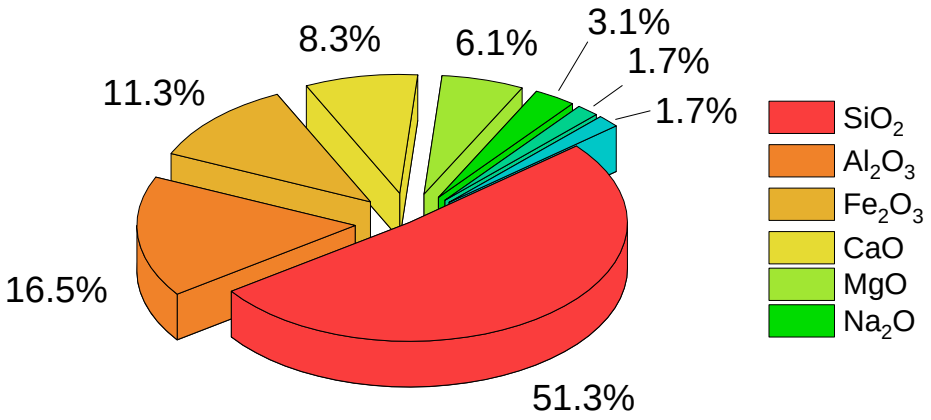


**Figure 1.** Chemical composition of basalt fibers [13].

In comparison to GFRP or CFRP, the number of publications providing data of mechanical properties of BFRP is small, see References [14,15] for a review. A similar material with a different experimental program was investigated by Davis et al. [16]. Specifically, for unidirectional BFRP made with epoxy-based prepregs in industrial processing quality, no detailed study is available. To resolve this issue, we perform a comprehensive quasi-static mechanical characterization of such a material, including tensile, compressive and shear tests, parallel and perpendicular to the fiber direction, according to the current standardized test procedures for fiber reinforced polymers.

The remainder of this paper is organized as follows—we first introduce the materials and testing setup utilized in this work. Then, our results for the mechanical properties of BFRP are presented. We conclude with a critical review of our work and a classification of the present BFRP to other comparable FRPs.

## 2. Materials and Methods

### *2.1. Material and Specimen Geometry*

Laminated composite sheets were provided by INCOTELOGY GmbH, Pulheim, Germany. The composites are made from prepregs of basalt fibers with filament diameter 17 µm. The Youngs' modulus of the bare fibers according to ASTM-D2101 [17] is 92 GPa as reported by the manufacturer. The fiber areal weight is 300 g/m$^2$, and a low-viscosity epoxy resin system CP003 (prepreg identifier: CM-Preg T-B- 300/280 CP0031 32) by c-m-p GmbH 52525 Heinsberg, Germany, was used. The fiber surface was treated with a hydrophobic epoxysilane, 3-(2,3-Epoxypropoxy)propyl]-trimethoxysilanepoxysilane, to increase interfacial strength with the matrix, as suggested in Reference [18]. The composite was cured in an autoclave process: 30 min ramp time from ambient conditions to 120 °C and 3 bar overpressure; 120 min plateau; 30 min ramp down to ambient conditions. This resulted in a fiber volume density of 60%. The quality was checked with ultrasonic C-scanning, revealing no porosities. Three different layups are used in this work: unidirectional (UD) with thickness 2 mm, orthogonal $[\pm 45]_{2S}$ with thickness 2 mm, and quasi-isotropic (QI) $[0/\pm 45/90]_s$ with thickness 1.6 mm.

Test specimens were cut from these sheets using a diamond coated saw blade to obtain a good edge surface finish. For tensile testing, the regular specimen size according to ASTM D 3039 [19] is used. For compressive testing, the recommendations of EN ISO 14126 [20] are followed. The actual dimensions of the specimens are reported in Table 1 and Figure 3. The thickness and width of each specimen were measured at three positions and the average was used for computing the cross section as required for engineering stress evaluation. To prevent damage of the tensile specimens due to the grips of the testing machine, tabs made of a ±45 glass-fiber/epoxy laminate were glued to the ends using a 2-component epoxy resin adhesive (UHU Plus Endfest 300).

**Table 1.** Dimensions of the testing specimens in mm. $L_0$ denotes gauge length. For tensile testing, specimen sizes are according to ASTM D 3039 and for compressive testing based on ISO 14126.

| **Tension Specimen** | **Length mm** | **Width mm** | **Thickness mm** | **$L_0$ –** | **Layers** |
|---|---|---|---|---|---|
| 0° | 200.0 | 25.0 | 2.0 | 80.0 | 10 |
| 90° | 200.0 | 25.0 | 2.0 | 80.0 | 10 |
| shear | 200.0 | 25.0 | 2.0 | 80.0 | 10 |
| QI | 200.0 | 25.0 | 1.6 | 80.0 | 8 |
| **Compression Specimen** | | | | | |
| 0° | 110.0 | 10.0 | 2.0 | 10.0 | 10 |
| 90° | 110.0 | 10.0 | 2.0 | 10.0 | 10 |

### *2.2. Mechanical Characterization Setup*

Six different load cases were considered—tension and compression, parallel and perpendicular to the fiber direction, a ±45° tension case for shear properties, and tensile loading of the quasi-isotropic laminate along the main 0° fiber direction. A Zwick Roell Z100 universal testing machine equipped with a 100 kN load cell of accuracy class 1 in displacement control mode was used, see Figure 2. The displacement velocity was set to 2 mm/min and a total of 5 valid tests were performed for each load case. A test was only considered valid if failure occurred within the gauge section.

For the tensile tests, longitudinal strain was measured using a clip-on extensometer with a gauge length of $l_0 = 30$ mm. Young's Modulus was determined from the slope of the engineering stress/strain curve in the strain interval $\varepsilon_1 = 0.05\%$ and $\varepsilon_2 = 0.25\%$. Poisson's ratio was determined using Digital Image Correlation (DIC). To this end, a fine speckle pattern was applied to the surface of the specimen using an airbrush spray gun: after coating the gauge section with a white layer, black speckles were sprayed with a 0.35 mm nozzle and acrylic ink (Schmincke, Aero Color Professional), see Figure 3A. For DIC, images were recorded using a high-resolution camera (Blackmagic Production Camera 4K, 4000 × 2160 pixels, Canon EF 100 mm f/2.8 Macro USM lens, see Figure 2). A commercial evaluation software (GOM Correlate) was used to evaluate the displacement field and compute the strains. Poisson's Ratio was evaluated in the range of $\varepsilon_{p1} \in [0.1\%, 0.3\%]$, according to testing standard ASTM D 3039. The DIC setup was validated by checking that the longitudinal strain from the mechanical extensometer agrees with the longitudinal strain determined by DIC.

The in-plane shear properties of the BFRP laminate was inferred from tensile testing of ±45° specimens according to ISO 14129 [21]. Shear stress is calculated from $\tau_{12} = \frac{F}{2A}$, where $F$ is tensile load and $A$ is the specimen's cross section area. Shear strain $\gamma_{12} = \varepsilon_x - \varepsilon_y$ is the sum of axial and transversal strain $\varepsilon_x$ and $\varepsilon_y$. The shear modulus of elasticity is $G_{12} = \frac{\tau''_{12} - \tau'_{12}}{\gamma''_{12} - \gamma'_{12}}$, which represents the slope of the shear stress/strain-curves shown in Figure 4C evaluated within the interval of $\gamma'_{12} = 0.1\%$ to $\gamma''_{12} = 0.5\%$.

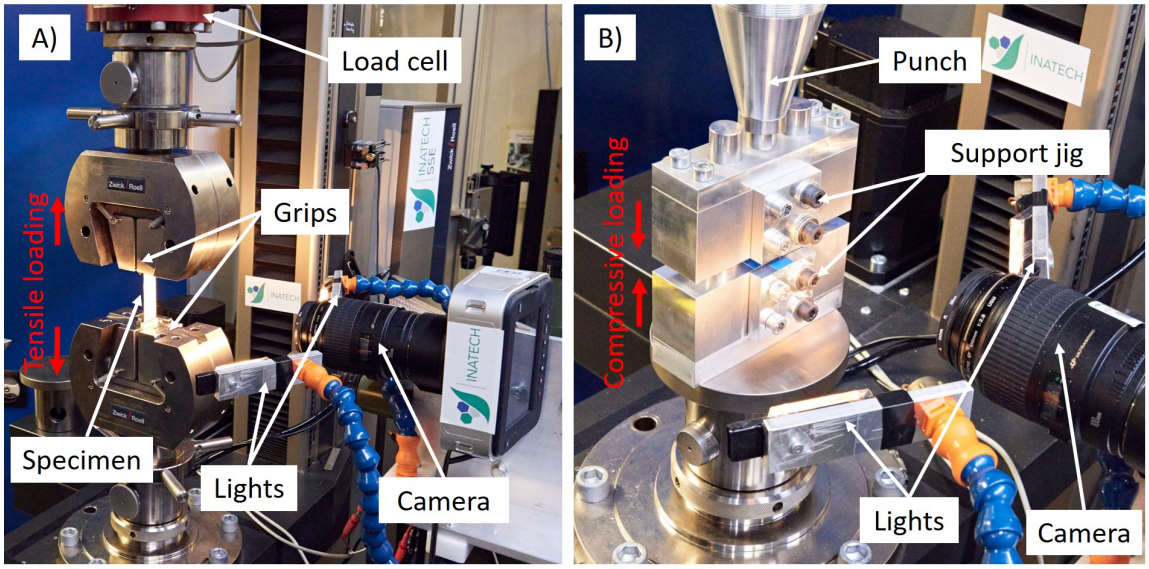


**Figure 2.** (**A**) For tensile and shear tests, the specimen is placed in the self-locking grips of the Zwick Roell Z100 universal testing machine. A high resolution camera captures the specimens' deformation for Digital Image Correlation (DIC) evaluation. (**B**) For compressive testing, a specimen support jig is centered under a punch, and strain gauges are employed.

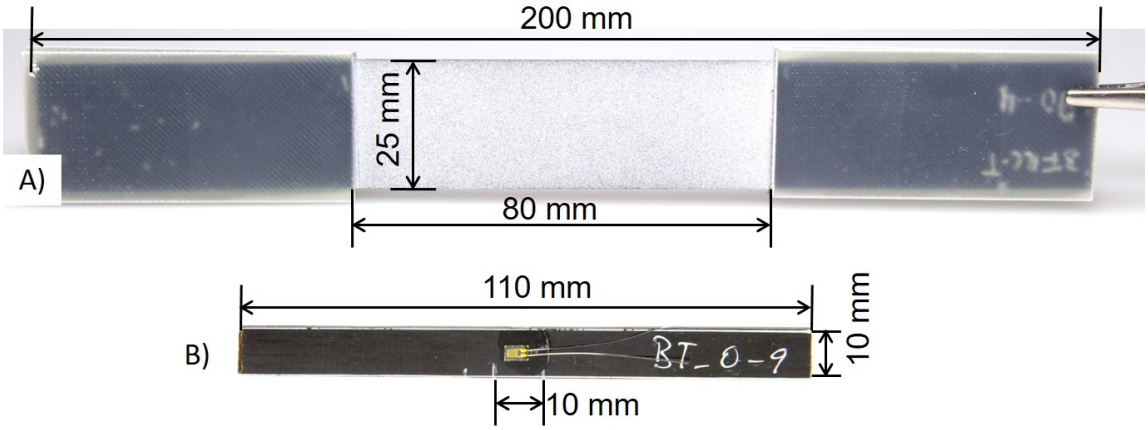


**Figure 3.** (**A**) Specimen for tensile and shear testing.The gauge section is coated with a fine speckle pattern for Poisson's ratio estimation. Glass–fiber tabs were bonded at both sides at the grip section. (**B**) Specimen for compressive testing with strain gauge.

The testing procedure for compressive testing was carried out according to ISO 14126 [20], with an end loading specimen support jig described under procedure 2 in this standard. Metal foil strain gauges were glued to both sides of the specimen to facilitate strain measurement and to detect buckling instabilities. Those specimens which showed buckling were considered invalid and removed from subsequent analysis.

For each testing series, an average was computed following the procedure described in Reference [22].

## 3. Results

### 3.1. Mechanical Characterization of BFRP

The resulting stress/strain-graphs of the tension, shear, and compression tests are shown in Figure 4. Table 2 lists the mechanical properties and engineering parameters gained from these experiments. In Figure 5 the different failure modes are shown, which result from their respective fiber lay-ups.

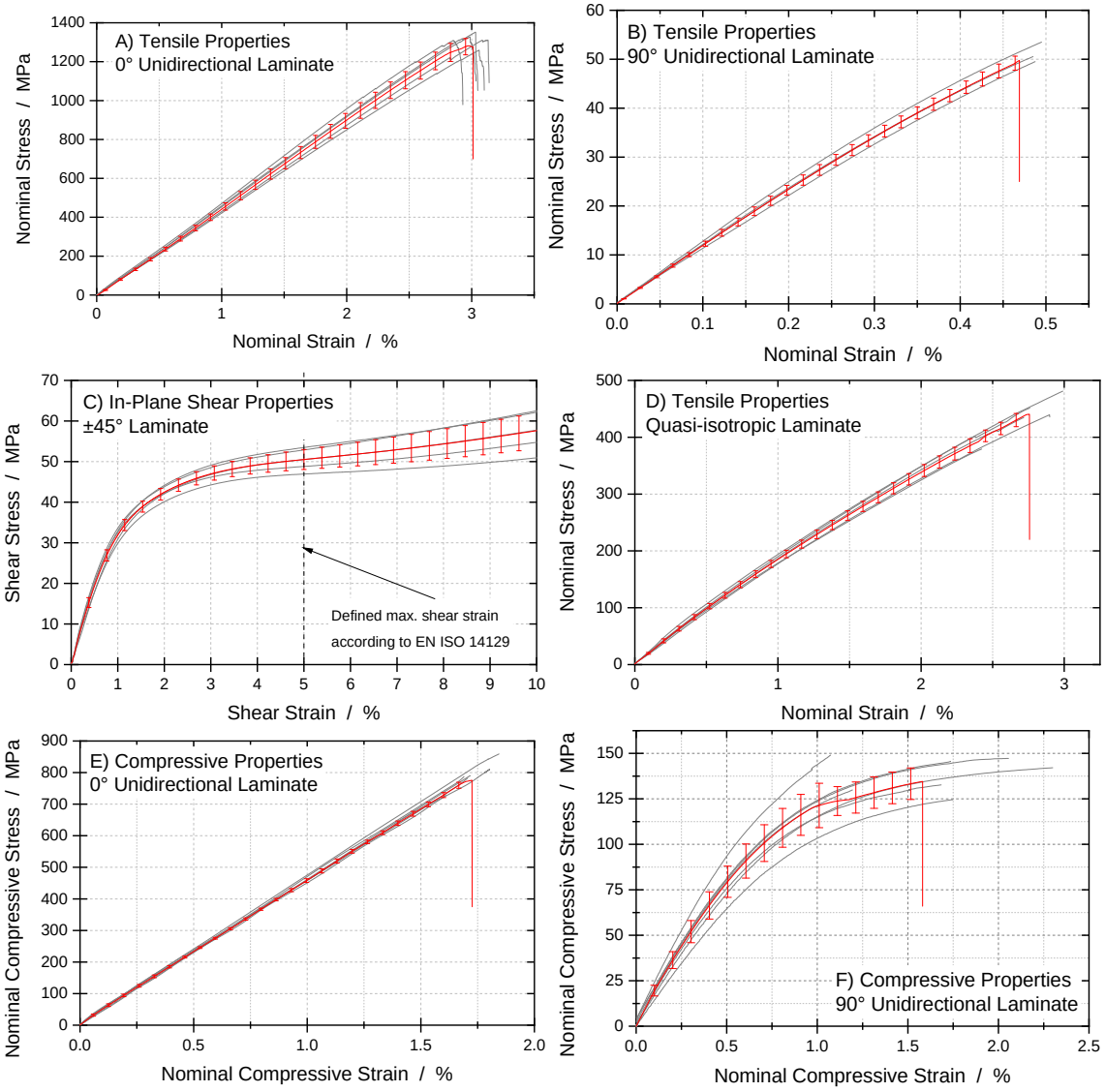


**Figure 4.** Tensile and compressive stress/strain behaviour of the unidirectional basalt/epoxy polymer. The red curve represents the average of the individual tests (grey lines). Vertical error bars represent the standard deviation of the average curve.

#### 3.1.1. Tensile Tests Parallel to the Fiber Direction—0°

Stress/strain-curves of the specimens in Figure 4A show a characteristic, almost perfectly linear slope until failure. The Young's modulus was evaluated to $E_{||} = 44.3 \pm 2.3$ GPa and the tensile strength as $\sigma_{||} = 1310 \pm 43$ MPa. A failure pattern which is typical for unidirectional laminates occurs as sudden failure of the fibres along with a strong release of stored elastic energy at a strain of $\varepsilon = 3.1 \pm 0.1\%$. Figure 5A shows the failure behaviour, characterized by an explosion-like bursting of the material.

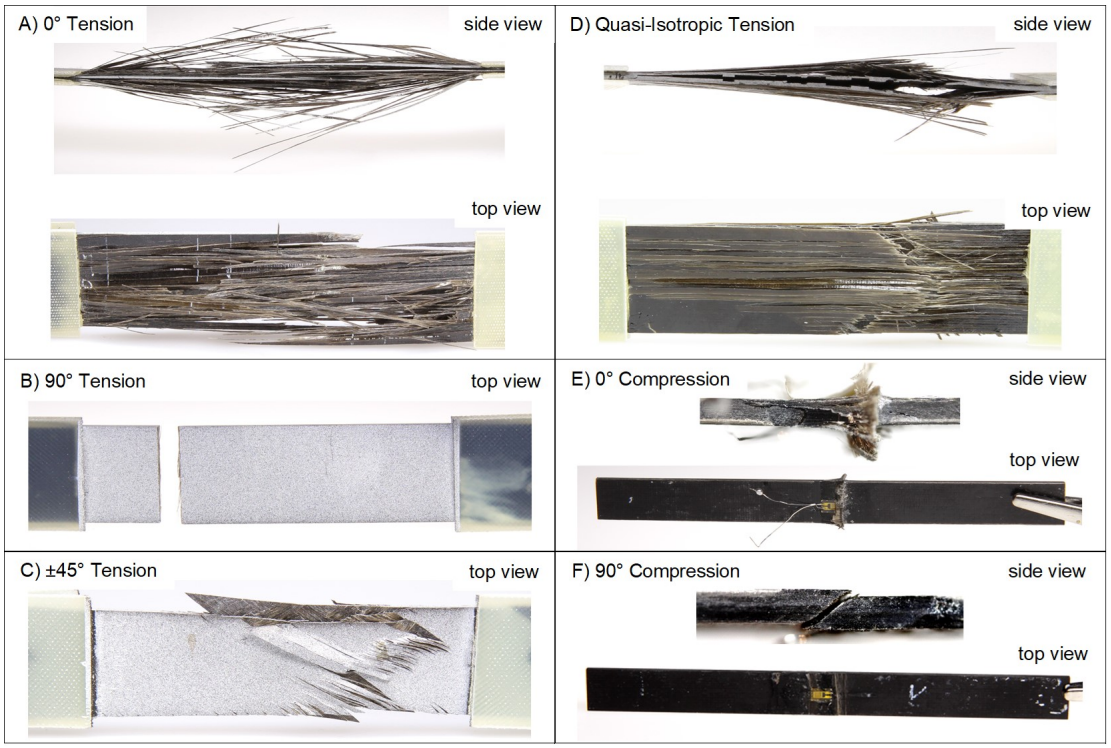


**Figure 5.** The different laminates exhibit characteristic failure modes: (**A**) 0° tension, (**B**) 90° tension, (**C**) ±45° tension, (**D**) quasi-isotropic tension, (**E**) 0° compression, (**F**) 90° compression

#### 3.1.2. Tensile Tests Perpendicular to the Fiber Direction—90°

In this case, the axis of loading is perpendicular to the fiber direction. Similar to the 0° case, the stress/strain-curves of the specimens exhibit a characteristic, mostly linear behaviour until sudden failure, see Figure 4B. The Young's modulus was evaluated to $E_{\perp} = 11.9 \pm 1.2$ GPa, and the tensile strength as $\sigma_{\perp} = 49.8 \pm 5.5$ MPa. Brittle failure occurs at $\varepsilon_{\perp} = 0.5 \pm 0.1\%$, see also Figure 5B. These results are similar to other unidirectional fiber-reinforced composites with epoxy matrix [23]. Major Poisson's ratio defined as $\nu = -\frac{\varepsilon_{\perp}}{\varepsilon_{\parallel}}$ was computed from these tests as $\nu = 0.27 \pm 0.03$.

#### 3.1.3. ±45° Tension Test—In-Plane Shear Modulus and Shear Strength

According to the testing standard of the in-plane shear tests with ±45° Laminates (ISO 14129 [21] and ASTM D3518 [24]), the stress/strain curves are to be truncated at $\gamma = 5\%$ shear strain. The $\gamma = 5\%$ point is considered to be the maximum shear strain with its corresponding maximum shear stress, which is $\tau_{12} = 50.5 \pm 2.5$ MPa. The shear stress/strain-curves of the specimens in Figure 4C exhibit an initially linear region with a slope of $G_{12} = 3.73 \pm 0.29$ GPa. A specimen, elongated to ≈10% elongated is shown in Figure 5C.

#### 3.1.4. Quasi-Isotropic Laminate Configuration—Tensile Properties

To determine the inter-laminate shear and bonding properties of the current BFRP material, a quasi-isotropic laminate was tested in tension. The laminate lay-up is a common and widely used system with 8 plies according to $[0/\pm 45/90]_s$. The resulting stress/strain-graph exhibits almost linear behaviour with a brittle failure pattern. The ultimate tensile strength is $\sigma_{QI} = 441 \pm 33$ MPa at a failure strain of $\varepsilon_{QI} = 2.8 \pm 0.2\%$, see Figure 4D and Table 2. Failure occurred in a sudden burst, where the failed 0° fibers thicken the specimen, see Figure 5D.

**Table 2.** Mechanical properties of continuous unidirectional and multidirectional basalt fiber reinforced epoxy laminates. Experiments were conducted based on current standards for testing of fiber reinforced composites as ASTM D 3039 (tension), EN ISO 14126 (compressive) and ISO 14129 (in-plane shear).

| **Tensile Properties Standard Size** | | |
|---|---|---|
| Ultimate Tensile Strength 0° | $1310 \pm 34$ | MPa |
| Ultimate Tensile Strain 0° | $3.1 \pm 0.1$ | % |
| Ultimate Tensile Strength 90° | $49.8 \pm 5.5$ | MPa |
| Ultimate Tensile Strain 90° | $0.47 \pm 0.09$ | % |
| Ultimate Tensile Strength QI | $441 \pm 33$ | MPa |
| Ultimate Tensile Strain QI | $2.8 \pm 0.2$ | % |
| Young's Modulus 0° | $44.3 \pm 2.3$ | GPa |
| Young's Modulus 90° | $11.9 \pm 1.2$ | GPa |
| Effective Y. Modulus QI | $20.3 \pm 1.6$ | GPa |
| Ultimate Shear Strength | $50.5 \pm 2.5$ | MPa |
| Ultimate Shear Strain | $0.05 \pm$ - | % |
| Shear Modulus | $3.73 \pm 0.29$ | GPa |
| Major Poisson's Ratio | $0.27 \pm 0.03$ | - |
| **Compressive Properties Standard Size** | | |
| Ultimate Compressive Strength 0° | $776 \pm 25$ | MPa |
| Ultimate Compressive Strain 0° | $-1.7 \pm 0.07$ | % |
| Ultimate Compressive Strength 90° | $135 \pm 6$ | MPa |
| Ultimate Compressive Strain 90° | $-1.6 \pm 0.6$ | % |
| Compressive Y. Modulus 0° | $46.2 \pm 2.4$ | GPa |
| Compressive Y. Modulus 90° | $15.2 \pm 1.8$ | GPa |

#### 3.1.5. Compressive Properties Parallel to the Fiber Direction—0°

The recorded stress/strain-graphs exhibit a linear stress/strain behaviour until brittle failure of the material occurs, see Figure 4E. This is a typical behaviour, due to the linear stiffness of the fiber. The compressive Young's modulus was determined as $E_{\parallel} = 46.2 \pm 2.4$ GPa with an ultimate strength of $\sigma_{\parallel} = 776 \pm 25$ MPa and a failure strain of $\varepsilon_{\parallel} = -1.70 \pm 0.07\%$. The 0° failure mode is characterized through the slide of plies into each other, a typical axial splitting mode [25], see Figure 5E.

#### 3.1.6. Compressive 90° Properties Perpendicular to the Fiber Direction

The compressive stress/strain-curves show an initially linear behaviour for the first half of the test, followed by a decreasing slope until failure, see Figure 4F. This behaviour is characteristic for fiber reinforced composites perpendicular to the fiber direction, see for example, Reference [26], due to nonlinear shear behaviour of the matrix. The compressive Young's modulus was determined as $E_{\perp} = 15.2 \pm 1.8$ GPa with an ultimate strength of $\sigma_{\perp} = 135 \pm 6$ MPa and a failure strain of $\varepsilon_{\perp} = -1.6 \pm 0.6\%$. Failure of the specimen exhibits a typical shear failure mode [25], see Figure 5F.

### *3.2. SEM Observations*

A sample of the BFRP shear test (±45° laminate) was investigated in a ZEISS EVO15 Scanning Electron Microscope (SEM). The backscattered electron images provide a good contrast between basalt-fibers (high atomic number, bright) and the polymer matrix (low atomic number, dark), see Figure 6. The focus was aligned on the fractured surfaces, to investigate the fiber-matrix bonding capabilities. Figure 6A shows wide areas of a complete bare fiber layer, with no remaining matrix and large areas, covered with a thick matrix layer. A closer look onto single fibers (B) also indicates no existent matrix leftovers. In the matrix layer, smooth fiber debonding marks are present (C). This observations suggest that the fiber/matrix interface is weak and easy to debond [27].

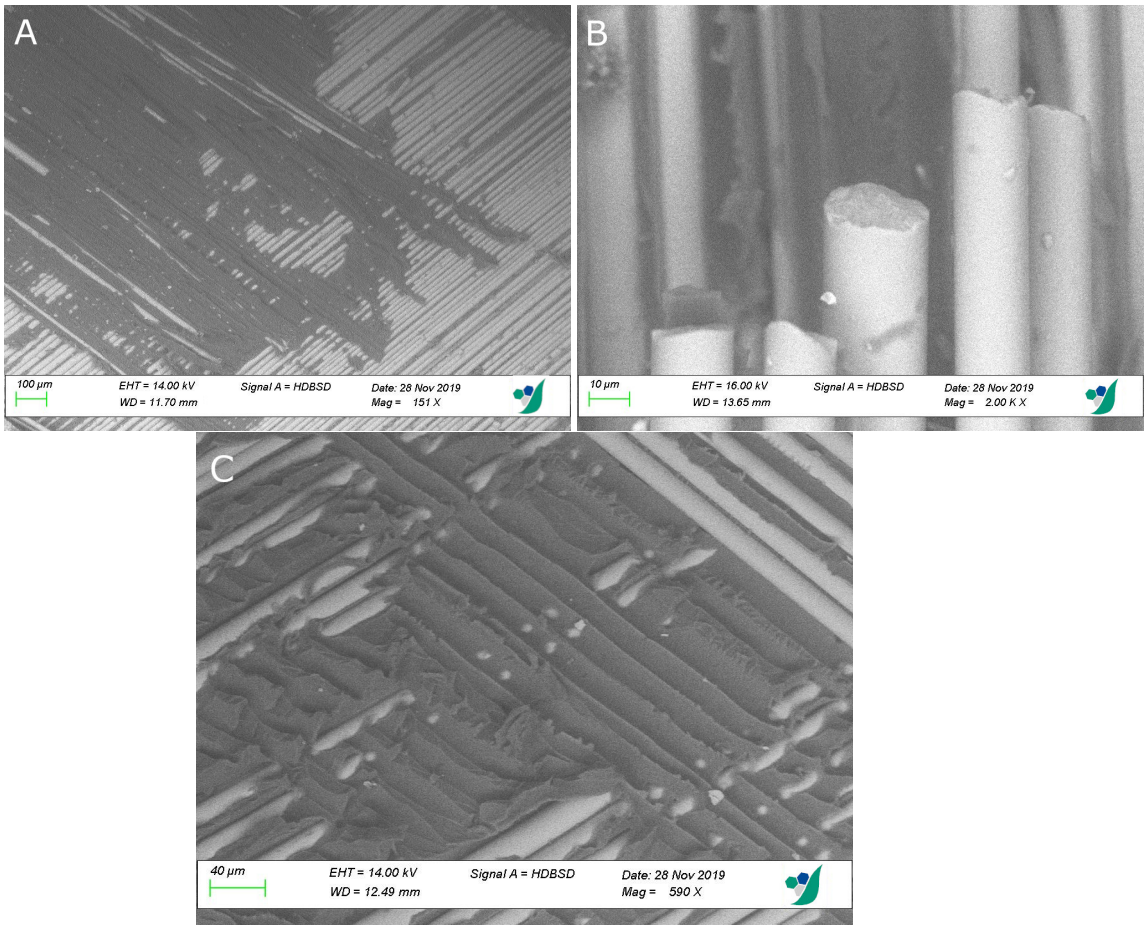


**Figure 6.** Scanning Electron Microscope (SEM) images of the fractured shear sample show large areas of bare fibers (**A**) and, on a closer look, bare fibers without matrix leftovers (**B**). These results indicate, together with the fiber debonding marks in (**C**), that the fiber-matrix interface is weak.

## 4. Discussion

In general, the experimental results described in Section 3 indicate that the mechanical performance of BFRP is comparable to similar composites containing glass fibers. However, BFRP performs less well than comparable carbon fiber composites, see Figure 7 for details. We note that, for the following comparison, typical, or average, carbon/glass fiber composite data is taken from existing reviews. We cannot compare against otherwise identical composites, because the resin system, the fiber treatment, and production parameters are different. Therefore, this comparison must be understood rather qualitatively.

With respect to glass fibers, both stiffness and strength in tension loading along the 0° direction are more similar to E-glass composites than to S-glass composites, see Figure 7B. In compression along the fiber direction, this finding is reversed with BFRP performing better than S-glass fiber composites, see Figure 7D.

The failed specimens, see Figure 5, exhibit typical failure modes for UD fiber composites—when loading along the fiber direction, both in tension and compression, the fibers fail. For loading perpendicular to the main fiber direction, matrix failure occurs. Shear failure is characterized by a pronounced plateau in the stress/strain-curve. The quasi-isotropic laminate fails with a sudden burst of the 0° layers at an elongation of 2.8%. Presumably, the inner 90° layers are already damaged before (see Figure 4B), but this does not affect the linearity of the stress/strain graph significantly.

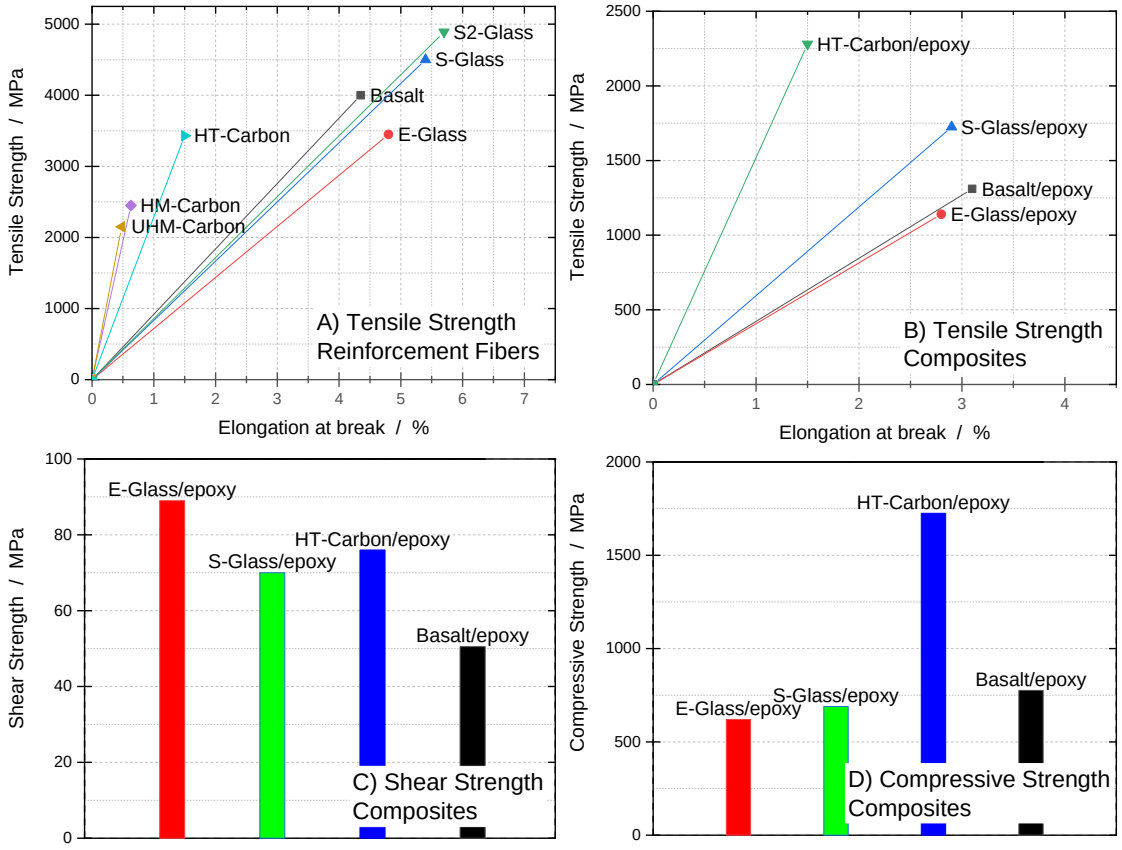


**Figure 7.** Typical mechanical properties of basalt, carbon and glass fibers and their unidirectional (UD) epoxy composites. Basalt/epoxy results stem from the present study, other fiber and composite properties are taken from Reference [28–31]. (**A**) Tensile strength of common reinforcement fibers, (**B**) Tensile strength of different fiber/epoxy composites (UD, tensile loading in 0° direction). (**C**) Shear strength and (**D**) Compressive strength of fiber/epoxy composites.

The rule-of-mixture is only roughly fulfilled by the observed 0° tensile stiffness—with the known fiber stiffness of 92 GPa, the epoxy matrix stiffness of 3.5 GPa, and a fiber volume fraction of 60%, a stiffness of 56.6 GPa is predicted. However, we have measured a stiffness of 44 GPa. We are currently unable to explain this mismatch. The measurements of the Young's moduli are deemed accurate and consistent, as the predicted stiffness for the QI specimen by classical laminate theory, using the values of the 0° and 90° samples results in an effective Young's Modulus of 21.7 GPa. This agrees well with the experimentally measured value of 20.3 GPa, see Table 2.

The compressive strength perpendicular to the fibers is 135 ± 6 MPa, which compares to for example, 128 MPa for epoxy/E-Glass fiber composite [30]. For shear loading, the BFRP composite considered here only reaches ≈60% of the strength of typical E-glass composites, indicating premature failure of the fiber/matrix interface, see Figure 7C. This is also supported by the SEM investigation of the fractured shear sample and could potentially be considerably improved on by further modifying the fibers' surface properties. Thus, our findings suggest that the basalt epoxy composite investigated here still requires improvements in the fiber-matrix adhesion, as indicated by the low shear strength. Potential interface improvements are discussed in Reference [18]. It seems that fiber surface modification using epoxysilane treatment is the most promising route.

## 5. Conclusions

This work presents a comprehensive characterization of the baseline material properties of a high-performance basalt composite composed of unidirectional plies of endless fibers within an epoxy matrix. Tension, shear, and compression experiments were performed under quasi-static conditions along, and perpendicular to the main fiber direction. While a number of similar studies is available for woven or braided basalt composites, this work is the first comprehensive investigation for a unidirectional basalt composite, produced in an industry-quality autoclave process. A study of 0° and 90° fiber lay-up samples of a comparable material system, produced in a hand-layup technique, shows similar results [32]. However, the 0° laminate autoclave prepreg samples investigated here achieve higher average ultimate strength and smaller standard deviations. This is presumably due to the higher production quality of the industrial autoclave process. At the same time it noted that the measured shear strength is significantly smaller than for typical E-glass composites. SEM imaging revealed that the reduced shear strength is caused by premature failure of the fiber-matrix interface. The most promising route for improving the fiber-matrix interface is the fiber surface modification using epoxysilane treatment.

In summary, the BFRP material investigated here performs slightly better than E-glass composites, but still not as good as S-glass composites. Carbon fiber composites outperform basalt fiber composites significantly. However, the good thermal and corrosion stability properties of basalt, along with the lower manufacturing costs, make BFRP an interesting candidate for certain applications. These include reinforcing material in construction, high temperature-insulation of engine parts, fire protection, and containment in corrosive environments such as chemical processes [14,15]. Recommendations, which BFRP composites are suited for specific applications may be found in Reference [9].

**Author Contributions:** Conceptualization, D.P., G.C.G. and M.M.; methodology, D.P., G.C.G. and M.M.; software, G.C.G.; validation, D.P. and G.C.G.; investigation, D.P. and S.B.; resources, G.C.G. and S.H.; data curation, D.P. and G.C.G.; writing—original draft preparation, D.P.; writing—review and editing, D.P. and G.C.G.; visualization, D.P.; supervision, G.C.G.; project administration, G.C.G. All authors have read and agreed to the published version of the manuscript.

**Funding:** The authors thankfully acknowledge funding of this work by the Gips-Schüle Stiftung, Stuttgart, Germany. G. Ganzenmüller gratefully acknowledges funding from Carl-Zeiss Foundation, Germany, Grant Title *Skalenübergreifende Charakterisierung robuster funktionaler Materialsysteme*.

**Acknowledgments:** We sincerely thank Stefan Hiermaier for acquiring the funding and general supervision of our research group.

**Conflicts of Interest:** The authors declare no conflict of interest. The funders had no role in the design of the study; in the collection, analyses, or interpretation of data; in the writing of the manuscript, or in the decision to publish the results.

## References

1. Dorigato, A.; Pegoretti, A. Fatigue Resistance of Basalt Fibers-Reinforced Laminates. *J. Compos. Mater.* **2012**, *46*, 1773–1785. [CrossRef]
2. Lopresto, V.; Leone, C.; De Iorio, I. Mechanical Characterisation of Basalt Fibre Reinforced Plastic. *Compos. Part B Eng.* **2011**, *42*, 717–723. [CrossRef]
3. Yao, Y.; Zhu, D.; Zhang, H.; Li, G.; Mobasher, B. Tensile Behaviors of Basalt, Carbon, Glass, and Aramid Fabrics under Various Strain Rates. *J. Mater. Civ. Eng.* **2016**, *28*, 04016081. [CrossRef]
4. Dhand, V.; Mittal, G.; Rhee, K.Y.; Park, S.J.; Hui, D. A Short Review on Basalt Fiber Reinforced Polymer Composites. *Compos. Part B Eng.* **2015**, *73*, 166–180. [CrossRef]
5. Colombo, C.; Vergani, L.; Burman, M. Static and Fatigue Characterisation of New Basalt Fibre Reinforced Composites. *Compos. Struct.* **2012**, *94*, 1165–1174. [CrossRef]
6. Lapena, M.H.; Marinucci, G.; Lapena, M.H.; Marinucci, G. Mechanical Characterization of Basalt and Glass Fiber Epoxy Composite Tube. *Mater. Res.* **2017**, *21*. [CrossRef]
7. Wu, G.; Wang, X.; Wu, Z.; Dong, Z.; Zhang, G. Durability of basalt fibers and composites in corrosive environments. *J. Compos. Mater.* **2015**, *49*, 873–887. [CrossRef]

8. Militký, J.; Kovačič, V.; Rubnerová, J. Influence of Thermal Treatment on Tensile Failure of Basalt Fibers. *Eng. Fract. Mech.* **2002**, *69*, 1025–1033. [CrossRef]
9. Liu, Q.; Shaw, M.T.; Parnas, R.S.; McDonnell, A.M. Investigation of Basalt Fiber Composite Aging Behavior for Applications in Transportation. *Polym. Compos.* **2006**, *27*, 475–483. [CrossRef]
10. Overkamp, T.; Mahltig, B.; Kyosev, Y. Strength of Basalt Fibers Influenced by Thermal and Chemical Treatments. *J. Ind. Text.* **2018**, *47*, 815–833. [CrossRef]
11. Hao, L.; Yu, W. Evaluation of Thermal Protective Performance of Basalt Fiber Nonwoven Fabrics. *J. Therm. Anal. Calorim.* **2010**, *100*, 551–555. [CrossRef]
12. Meyer, L.; Schulte, K.; Grove-Nielsen, E. CFRP-Recycling Following a Pyrolysis Route: Process Optimization and Potentials. *J. Compos. Mater.* **2009**, *43*, 1121–1132. [CrossRef]
13. Deák, T.; Czigány, T. Chemical Composition and Mechanical Properties of Basalt and Glass Fibers: A Comparison. *Text. Res. J.* **2009**, *79*, 645–651. [CrossRef]
14. Fiore, V.; Scalici, T.; Di Bella, G.; Valenza, A. A Review on Basalt Fibre and Its Composites. *Compos. Part B Eng.* **2015**, *74*, 74–94. [CrossRef]
15. Lebedev, M.P.; Startsev, O.V.; Kychkin, A.K. The effects of aggressive environments on the mechanical properties of basalt plastics. *Heliyon* **2020**, *6*, e03481. [CrossRef] [PubMed]
16. Davies, P.; Verbouwe, W. Evaluation of Basalt Fibre Composites for Marine Applications. *Appl. Compos. Mater.* **2018**, *25*, 299–308. [CrossRef]
17. ASTM. *D2101: Standard Test Methods for Tensile Properties of Single Man-Made Textile Fibers Taken from Yarns And Tows*; American Society of Testing and Materials: West Conshohocken, PA, USA, 1994.
18. Varley, R.J.; Tian, W.; Leong, K.H.; Leong, A.Y.; Fredo, F.; Quaresimin, M. The effect of surface treatments on the mechanical properties of basalt-reinforced epoxy composites. *Polym. Compos.* **2013**, *34*, 320–329. [CrossRef]
19. ASTM. *D3039: Standard Test Method for Tensile Properties of Polymer Matrix Composite Materials*; American Society of Testing and Materials: West Conshohocken, PA, USA, 2000.
20. ISO. *14126: 1999-Fibre-Reinforced Plastic Composites. Determination of Compressive Properties in the In-Plane Direction*; International Organization for Standardization: Geneva, Switzerland, 1999.
21. ISO. *14129: Fibre Reinforced Plastics Composite-Determination of the In-Plane Shear Stress/Shear Strain Response, Including the In-Plane Shear Modulus and Strength by the +-45 Tension Test Method*; British Standard Institute: London, UK, 1998.
22. Ganzenmüller, G.C.; Plappert, D.; Trippel, A.; Hiermaier, S. A Split-Hopkinson Tension Bar study on the dynamic strength of basalt-fibre composites. *Compos. Part B Eng.* **2019**, *171*, 310–319. [CrossRef]
23. Sathishkumar, T.; Satheeshkumar, S.; Naveen, J. Glass Fiber-Reinforced Polymer Composites—A Review. *J. Reinf. Plast. Compos.* **2014**, *33*, 1258–1275. [CrossRef]
24. ASTM. *D3518: Standard Test Method for In-Plane Shear Response of Polymer Matrix Composite Materials by Tensile Test of a 45 Laminate*; American Society of Testing and Materials: West Conshohocken, PA, USA, 2001.
25. Carlsson, L.A.; Adams, D.F.; Pipes, R.B. *Experimental Characterization of Advanced Composite Materials*; CRC Press: Boca Raton, FL, USA, 2014. [CrossRef]
26. Zhou, H.W.; Yi, H.Y.; Gui, L.L.; Dai, G.M.; Peng, R.D.; Wang, H.W.; Mishnaevsky, L. Compressive Damage Mechanism of GFRP Composites under Off-Axis Loading: Experimental and Numerical Investigations. *Compos. Part B Eng.* **2013**, *55*, 119–127. [CrossRef]
27. Schoßig, M. *Schädigungsmechanismen in faserverstärkten Kunststoffen: Quasistatische und Dynamische Untersuchungen*; Vieweg+Teubner Verlag: Berlin, Geramny, 2011. [CrossRef]
28. Schürmann, H. *Konstruieren mit Faser-Kunststoff-Verbunden*, 2nd ed.; VDI-Buch; Springer: Berlin/Heidelberg, Germany, 2007.
29. Hausrath, R.L.; Longobardo, A.V. High-Strength Glass Fibers and Markets. In *Fiberglass and Glass Technology: Energy-Friendly Compositions and Applications*; Wallenberger, F.T., Bingham, P.A., Eds.; Springer US: Boston, MA, USA, 2010; pp. 197–225. [CrossRef]
30. Daniel, I.M.; Ishai, O. *Engineering Mechanics of Composite Materials*, 2nd ed.; Oxford University Press: New York, NY, USA, 2006.

31. Burgoyne, C.J.; Byars, E.; Guadagnini, M.; Manfredi, G.; Neocleous, K.; Pilakoutas, K.; Taerwe, L.; Taranu, N.; Tepfers, R.; Weber, A.; et al. *FRP Reinforcement in RC Structures*; fib Bulletin No. 40; The International Federation for Structural Concrete: Lausanne, Switzerland, 2007. [CrossRef]
32. Robert, C.; Pecur, T.; McCarthy, E.D.; Brádaigh, C. *Tidal Turbine Blade Composites Using Basalt Fibre Reinforced Powder Epoxy*; Engineers Australia: Barton, Australia, 2019; p. 3687.